# Mapping the Thermal Behavior of DNA Origami Nanostructures

Xixi Wei, Jeanette Nangreave, Shuoxing Jiang, Hao Yan, and Yan Liu*

Department of Chemistry and Biochemistry and Center for Single Molecule Biophysics, Biodesign Institute at Arizona State University, 1001 South McAllister Avenue, Tempe, Arizona 85287-5701, United States

S *Supporting Information*

ABSTRACT: Understanding the thermodynamic properties of complex DNA nanostructures, including rationally designed two- and three-dimensional (2D and 3D, respectively) DNA origami, facilitates more accurate spatiotemporal control and effective functionalization of the structures by other elements. In this work fluorescein and tetramethylrhodamine (TAMRA), a Förster resonance energy transfer (FRET) dye pair, were incorporated into selected staples within various 2D and 3D DNA origami structures. We monitored the temperature-dependent changes in FRET efficiency that occurred as the dye-labeled structures were annealed and melted and subsequently extracted information about the associative and dissociative behavior of the origami. In particular, we examined the effects of local and long-range structural defects (omitted staple strands) on the thermal stability of common DNA origami structures. The results revealed a significant decrease in thermal stability of the structures in the vicinity of the defects, in contrast to the negligible long-range effects that were observed. Furthermore, we probed the global assembly and disassembly processes by comparing the thermal behavior of the FRET pair at several different positions. We demonstrated that the staple strands located in different areas of the structure all exhibit highly cooperative hybridization but have distinguishable melting temperatures depending on their positions. This work underscores the importance of understanding fundamental aspects of the self-assembly of DNA nanostructures and can be used to guide the design of more complicated DNA nanostructures, to optimize annealing protocol and manipulate functionalized DNA nanostructures.
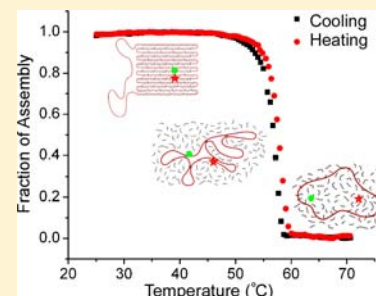
INTRODUCTION

DNA nanotechnology is a rapidly evolving field that exploits the unique properties of DNA for nanoscale engineering. In particular, DNA origami technology has attracted considerable attention for a variety of applications.[1−3] DNA origami is a technique in which a long single stranded viral genome (referred to as a scaffold, generally derived from the M13mp18 bacteriophage) is folded into predefined two- and three-dimensional (2D and 3D, respectively) structures through interactions with a large number of short DNA oligonucleotides (staples).[4−6] The unique features of DNA origami, e.g., addressability at each staple position, high pixel density, and nanometer-scale resolution, make the precise organization of selected biomolecules and nanoparticles possible. The potential applications of DNA nanoarchitectures continued to expand with the construction of increasingly complex DNA origami structures.[7,8]

Achieving more advanced DNA origami designs and effective functionalization by other biomolecules and nanoparticles is likely to require a deeper understanding of the thermodynamic properties and behavior of the DNA origami platform.[9] Several previous studies examined the assembly and disassembly of DNA nanostructures, based either on the change in ultraviolet (UV) absorbance that occurs upon formation of double-helical secondary structure or by means of a nucleic acid stain (SYBR green) that can detect the presence of single- and double-stranded DNA.[9−12] However, these methods suffer from limited accuracy, and detailed information about the local

structure and dynamic behavior of the DNA origami cannot be determined from global average measurements. Song et al. used an atomic force microscope (AFM) to visualize the transformation of a DNA origami structure which exhibited a rough transition based on relatively coarse temperature control (1 °C/min). The experiments were conducted at a solid−liquid interface, and it is possible that the behavior of the origami in their study does not reflect that in solution. In addition, scanning the sample with an AFM probe is likely to disturb the structural integrity of the DNA nanostructures.[13] Recently, Sobczak et al. used real-time fluorometric monitoring and cryogenic reaction quenching to probe the thermal folding and unfolding of 3D DNA origami nanostructures. Their study revealed intriguing differences between the assembly and melting transitions, though at a global level.[14]

Förster resonance energy transfer (FRET) is a convenient way to monitor molecular association and dissociation events.[15,16] With FRET, the efficiency of energy transfer depends on several factors including the distance between the donor and the acceptor fluorophores. DNA origami is particularly compatible with FRET-based reporting, as adjacent staples can be easily functionalized with FRET dyes.[17,18] When the temperature is low, the origami structures are fully assembled and the FRET dyes are close together, resulting in efficient energy transfer. As the temperature increases the
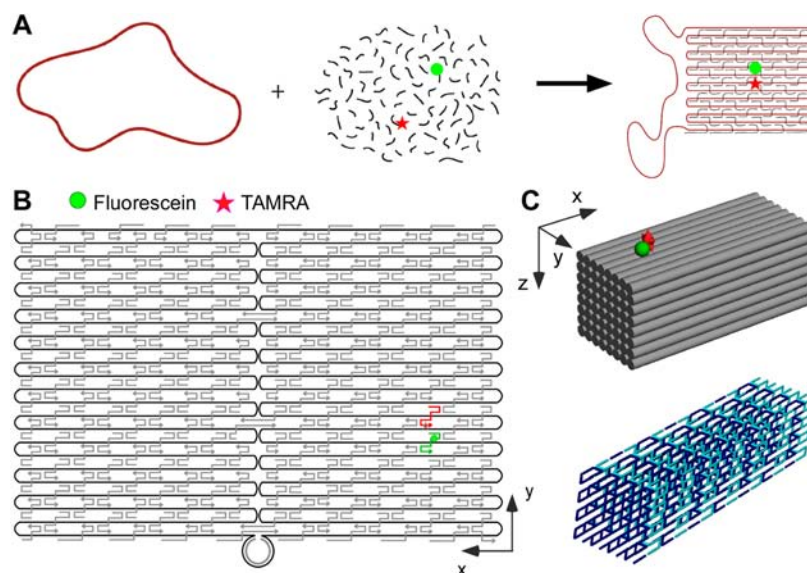
Figure 1. FRET-based monitoring of DNA nanostructure assembly and disassembly. (A) Schematic representation of the self-assembly of a DNA origami structure from a circular scaffold and collection of complementary staple strands. Two selected staples are modified with FRET donor (fluorescein, green circle) and acceptor (TAMRA, red star) dyes, respectively. (B) Rectangular DNA origami structure used to investigate assembly/disassembly in 2D. Note the position of the FRET dyes on different helical rows in the lower right-hand quadrant. (C) Cuboid DNA origami structure used to investigate assembly/disassembly in 3D. The upper diagram depicts a FRET pair on the top surface of the structure. The lower diagram shows the layer by layer staple organization (alternative layers are shown in dark and light blue).

structures destabilize and the dye-labeled strands begin to dissociate from the scaffold resulting in negligible energy transfer. FRET-based monitoring of DNA nanostructure assembly and disassembly can be used to overcome the technical barriers faced by UV absorption and DNA staining methods because the corresponding fluorescence energy-transfer events have no correlation with the presence of extra unlabeled DNA strands; thus, the background interference is minor which permits more accurate measurement. The behavior of each individual staple, including the dye-labeled strands, is highly cooperative, and it is reasonable to propose that FRET between two representative individual strands will reliably reflect the overall thermal behavior of the structure. On the other hand, FRET is sensitive enough to detect the nanometer scale changes in distance that are connected to underlying structural changes elicited by a variety of factors, including the presence or absence of structural elements in close proximity to the reporter molecules. This makes it possible to probe the behavior of very specific areas of the origami structure.[19,20]

We previously used a FRET-based strategy to study the thermodynamic behavior of small, interacting DNA tiles. The number and relative position of the sticky end connections between the tiles and the flexibility and rigidity of the core elements of the tiles themselves were systematically varied, and the effects on the thermal stability of the assembled structures were determined.[21,22] In the current study we used the same FRET method to reveal the global and local stability of more complex DNA origami structures. Initially, we established the thermodynamic characteristics of fully assembled 2D and 3D origami as signified by the transition temperature of representative staple—scaffold interactions. Next, we held the position of the FRET dyes constant as we induced defects in the origami structures (i.e., selective omission of staples) at various distances from the reporter molecules. The results allowed us to determine the effects of distant and local defects

on the stability of the origami in the vicinity of the reporter molecules. We further probed the effects of local defects on nanostructure stability by systematically removing individual staples or small groups of staples directly adjacent to the FRET dyes. Finally, we attempted to determine if the origami exhibit uniform stability across their entire structure or if different areas of the structure are more susceptible to destabilization. Here, the stability was examined when the reporter dyes were moved to different positions in the structure.

The FRET studies here reveal subtle details about the formation and dissociation of 2D and 3D DNA origami nanostructures that reflect both local and long-range factors. This work has allowed us to gain a deeper understanding of the thermodynamic behavior of DNA origami structures and the hybridization of individual staple strands to the scaffold at the molecular level.

Design of FRET-Labeled 2D and 3D DNA Origami. For each experimental design we selected two neighboring staple strands in the DNA origami structures and modified them with FRET donor (fluorescein) and acceptor (TAMRA) dyes, respectively, as shown in Figure 1A. The distance between the dyes in the fully assembled DNA origami is comparable to (or smaller than) the Förster distance (~5 nm), permitting observation of the changes in FRET efficiency that occur during the assembly/disassembly processes.[16,23] In addition, the donor and acceptor dye-labeled staples were designed to bind to different segments of the scaffold (i.e., different helices in the final product) to report on global structural changes. Assembly and disassembly of the DNA origami structures were induced by ramping the temperature up and down. At very high temperatures the FRET efficiency is low because the dye-labeled staples are dissociated from the scaffold and are relatively far apart. As the temperature is decreased, the dye-labeled strands begin to associate with the scaffold and are close together in the final product, thus the FRET efficiency is relatively high.
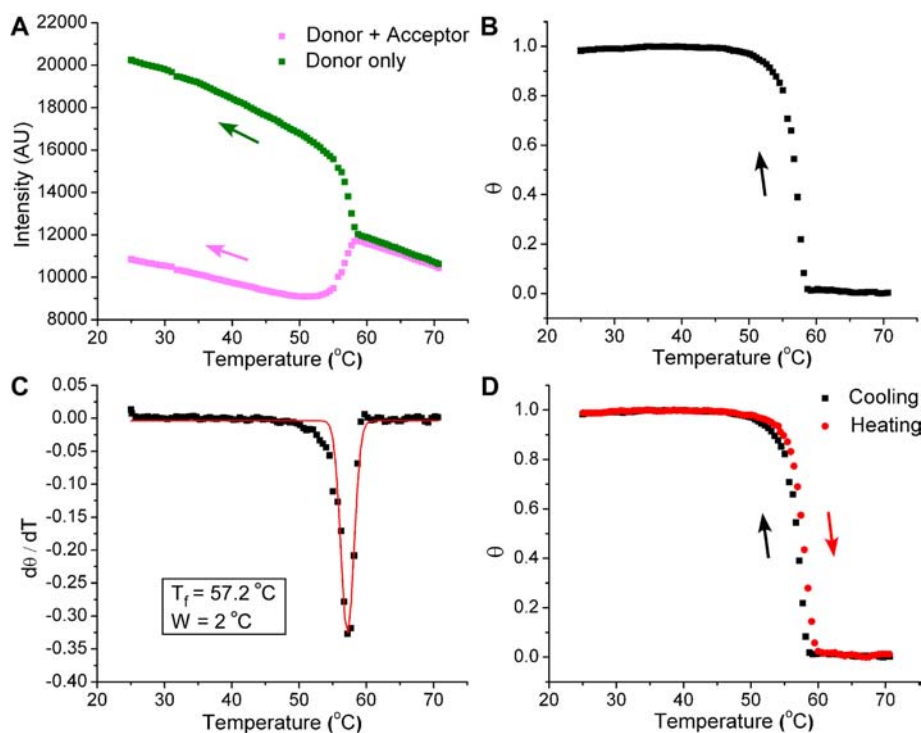
Figure 2. Procedure to determine the transition temperatures of DNA origami structures. All data presented in this figure correspond to the unmodified, rectangular DNA origami reference structure. Each sample was heated at 95 °C for 5 min, and the fluorescence emission of fluorescein at 522 nm was monitored with 492 nm excitation. For rectangular origami, the temperature was reduced from 80 to 25 °C at 0.1 °C/min for the cooling cycle and vice versa for the heating cycle. For cuboid origami, the temperature was reduced at 0.1 °C/min from 80 to 75 °C, 0.1 °C/2 min from 75 to 65 °C, 0.1 °C/3 min from 65 to 40 °C, and 0.1 °C/2 min from 40 to 25 °C for the cooling cycle and vice versa for the heating cycle. (A) Plot of the fluorescent emission of fluorescein (donor) versus temperature. The data were collected during the assembly phase (cooling), with the green and pink traces corresponding to the donor-only and fully assembled donor−acceptor structures, respectively. The arrows indicate the direction of the cooling temperature sweep. (B) Normalized FRET efficiency (θ) of the same sample as a function of temperature. The arrow indicates the cooling temperature sweep. (C) Plot of the first derivative of the data shown in (B) as a function of temperature. The curve is fitted by a Gaussian function to identify the transition temperature (T_f) and the width of the transition (W). (D) Overlay of the normalized FRET efficiency plots corresponding to cooling (black) and heating cycles (red) that reveals the reversible assembly and disassembly of the structure. The arrows indicate the direction of temperature sweep (black for cooling and red for heating).

We selected a common rectangular design (24 parallel helices) to investigate the thermodynamic behavior of 2D DNA origami (Figure 1B).[4] Here, most staples are 32 nucleotides (nt) long and can be divided into three consecutive domains (8, 16, and 8 nt) that bind to unique regions of the scaffold, respectively, bridging three adjacent helices. As shown in Figure 1, the donor and acceptor dye-modified staples are designed to bind to the scaffold such that they bring the FRET pair into close proximity upon formation of the origami structure. Figure 1B depicts one of three FRET dye positions that were analyzed.

We also explored the thermodynamic behavior of a 3D DNA origami cuboid structure composed of 8 × 8 helices bound in a square lattice.[24] In this design, the staples are grouped into 14 layers along the helical axis (x direction). Four different FRET dye positions were investigated, including the one depicted in Figure 1C. For all 2D and 3D designs (Figures 5 and 6), the distance between the donor and the acceptor dye is estimated to be ∼3−5 nm in the fully assembled structure.

Data Analysis. The fluorescence thermal curves were measured using a PCR thermocycler (MX3005P, Stratagene) capable of monitoring the real-time change in fluorescence of the reporter dyes as a function of temperature. For all the nanostructures investigated, two samples were prepared with identical experimental conditions: one sample contained both the donor (fluorescein) and acceptor (TAMRA) dyes, whereas the second sample contained only the donor fluorophore and the corresponding unlabeled acceptor oligomer as the reference (Figure 2A). This scheme allowed for the measurement of the decrease in fluorescein emission resulting from energy transfer to TAMRA to calculate the FRET efficiency (Figure 2B).

The fluorescence of the donor (in the absence of the acceptor) gradually increased as the sample was cooled from 80 °C, until a rapid increase in fluorescence was observed at 57−58 °C (dotted green trace in Figure 2A). This sharp change in the fluorescence intensity of the donor was also observed during the heating cycle (e.g., Figure S4). The sharp transition observed in the donor-only sample is coincident with that observed in the fully assembled donor−acceptor sample (pink dotted trace in Figure 2A), reflecting the temperature at which the dye-modified staples hybridize to the scaffold strand.

The nearly linear, temperature-dependent change in the fluorescence quantum yield of fluorescein that we observed has been reported previously.[25−27] However, the sharp increase in fluorescence intensity (∼ 40%) that occurred upon hybridization of the dye-modified staple cannot be explained by the temperature dependence of the dye. Pinheiro et al. recently reported a ∼30−40% increase in the fluorescence intensity of fluorescein upon formation of double-helical DNA adjacent to the site of the dye modification (5′ dye-labeled staple).[28] The increase in fluorescence was accompanied by a decrease in

anisotropy, indicating a reduced interaction between the dye and the neighboring DNA bases upon formation of double-helical DNA. Here, all dye modifications are at internal positions of staples and similarly, we anticipate that the interaction of the dye with adjacent nucleotides in the single-stranded DNA limits the exposure of the dye to the solvent, restricts its rotational dynamics, and contributes to quenching of its fluorescence. Hybridization of staples to the scaffold at positions adjacent to the dye modification is expected to release the dye from its interactions so that it gains exposure to a more polar environment and displays a significant increase in the quantum yield.

On the other hand, the fluorescence intensity of the donor is expected to undergo a dramatic decrease upon formation of the DNA origami structure, as the distance between the FRET pair in the fully assembled structure is small enough for efficient energy transfer to occur. Apparently, the FRET interaction dominates when the acceptor is present, as demonstrated by the data shown in Figure 2A (pink dots).

The FRET efficiency (E), which is related to the change in distance between the FRET donor and acceptor, is defined by the following equation:

$$E = (I_D - I_{DA})/I_D \tag{1}$$

where I_D and I_{DA} are the fluorescent intensity of the donor in the absence or presence of the acceptor, respectively. Assuming that the system is given adequate time to reach equilibrium at each temperature, the variation in FRET efficiency is expected to reflect any temperature-dependent structural changes. Consequently, normalized FRET efficiencies are proportional to the fraction of assembled structures (θ):

$$\theta = (E - E_{min})/(E_{max} - E_{min}) \tag{2}$$

where E_{min} represents the minimum FRET efficiency that is present when the structure is completely dissociated (high temperatures) and E_{max} represents the maximum FRET efficiency that is observed when the structures are fully assembled (low temperatures). Thus, FRET efficiency is normalized between 0 and 1 where "$\theta = 0$" represents the fully dissociated state, while "$\theta = 1$" indicates complete formation of the DNA origami.

From a plot of θ versus temperature T, we can identify the transitions that correspond to assembly or disassembly of the origami during the cooling and heating cycles, respectively (an example cooling profile is shown in Figure 2B). The transition observed during the cooling cycle is referred to as the temperature of formation (T_f), while the one observed during the heating cycle is referred to as the melting temperature (T_m). A plot of the first derivative of θ ($d\theta/dT$) versus temperature (T) is fit by a Gaussian function to yield the midpoints (T_f or T_m) and width (W) of the transition (Figure 2C). Overlaying the cooling and heating thermal curves for the same sample indicates the reversibility of the transition (Figure 2D).

The results of such an analysis can be used to understand more about the thermal behavior of 2D and 3D DNA origami structures. For example, the transition temperatures indicate the stability of the FRET-modified region, while the shape of the transition provides information about the cooperativity of staple hybridization. In general, higher transition temperatures reflect more stable interactions. Smooth, sharp transitions indicate rapid, cooperative assembly in which the system reaches equilibrium in a narrow temperature range. In addition, it is possible to follow the thermal characteristics of donor- and acceptor-modified staples separately to gain insight in the mechanism of annealing and melting at the molecular level.

■ RESULTS AND DISCUSSION

2D and 3D Reference Structures. First, the experimental and data analysis methods described above were used to determine the transition temperatures of a basic 2D and a 3D DNA origami structure (Figures S1 and S2 and Tables S1−S4). The transition temperatures (T_f and T_m) of the 2D rectangular origami structure are 57.2 ± 1.0 and 57.9 ± 1.3 °C, respectively (Figure 2D). The minimal discrepancy in temperature between the cooling and heating cycle transitions and the sharp features of the transitions reveal that the structure is reversibly assembled/disassembled at ∼57 to 58 °C. The data also indicates that the 2D origami structure forms and dissociates relatively rapidly such that the system can indeed be considered to be at equilibrium at each measurement temperature. We also demonstrated that the rates of temperature change in the cooling and heating cycles, for both 2D and 3D samples, are slow enough to ensure equilibrium at each temperature (Table S5).

However, clear hysteresis between the cooling and heating curves was observed for the 8 × 8 layer 3D cuboid origami structure (Figure 6A), with a T_f of 54.6 ± 1.3 °C and a T_m of 60.4 ± 1.4 °C (corresponding to the dye positions depicted in Figure 1C). We propose that the ∼6 °C difference between T_f and T_m is due to the complex folding interactions that occur between various layers in the structures, making the assembly process much slower than the melting process. A more detailed discussion of these results can be found in the Assembly in 3D section below.

Scaffold to Staple Ratio. Next, we wanted to confirm whether or not the ratio between the M13 scaffold and the staple strands has an effect on the thermal characteristics of the assembly/disassembly process. Typically, the molar ratio of the M13 scaffold to the staples is 1:5 for 2D origami and 1:10 for 3D origami. Here, we held the M13 to dye-modified staple ratio at 1:2 and evaluated 1:1 and 1:5 ratios of M13 to unmodified staples. We also performed other experiments in which we held the ratio of M13 to unmodified staples at 1:5, while we examined 1:1, 1:2, and 1:5 M13 to dye-modified staple ratios. The results of these experiments are listed in Table 1A.

The melting temperatures are very close in all cases; however, the temperature of formation is slightly reduced for experiments with a 1:1 ratio of M13 to staples. This result is expected because without excess staples to accelerate the hybridization and M13 scaffold folding processes, it takes longer to reach equilibrium at each temperature. In addition, any truncated staples in solution (the staples were not purified before use) can bind to the scaffold and lower the thermal stability, further reducing the T_f. When the ratio of the scaffold to the unmodified staples was kept constant (1:5) and the ratio of the scaffold to the dye-modified staples was varied, the T_f and T_m showed no significant difference. This result confirmed that the dye-modified staples and FRET-based method described here are reliable reporters of the thermal behavior in such a system. We used a 1:2 of M13 to dye-modified staples and a 1:5 of M13 to unmodified staples for all subsequent studies of the 2D DNA origami structure.

Note that the general practice when assembling the 2D rectangular structure used in these experiments is to omit the outermost layers of staples (adjacent to the ends of the helices on both sides) in order to reduce the nonspecific end to end

Table 1. The Effect of the Scaffold (M13) to Staple Ratios[a]

M13:FRET	M13:staples	cooling T_f (°C)	heating T_m (°C)
(A) Transition Temperatures Measured From 2D DNA Origami			
1:2	1:1	55.6 ± 0.9	57.6 ± 1.3
1:2	1:5	57.2 ± 1.0	57.9 ± 1.3
1:1	1:5	57.2 ± 0.9	57.7 ± 1.4
1:5	1:5	57.5 ± 0.9	58.3 ± 1.0
(B) Transition Temperatures Measured From 3D DNA Origami			
1:2	1:1	48.3 ± 3.3	57.9 ± 2.4
1:2	1:5	53.5 ± 1.2	60.0 ± 1.4
1:2	1:10	54.6 ± 1.3	60.4 ± 1.4
1:5	1:10	54.6 ± 1.1	60.9 ± 1.3
1:5	1:15	54.2 ± 1.5	60.4 ± 1.6

[a](A) No significant differences were observed for the 2D structure, except for a 1:1 ratio of M13 to staples which induced a T_f of 1 to 2 °C lower than the other cases. (B) No significant differences were observed in the 3D structure, except for a 1:1 ratio of M13 to staples where both the cooling and heating values are significantly lower. In all cases, a 6 to 7 °C difference between T_f and T_m was observed, except for a 1:1 ratio where a 9.6 °C difference was observed.

base stacking between structures. We measured the thermal transitions of the rectangular structure with and without the outermost staples and determined that the transition temperatures were nearly the same (0.1 to 0.3 °C difference for T_f and T_m, respectively) for both situations (Figures S4 and S5). For the sake of consistency and overall structural integrity, we included the outermost layers in the experiments described herein.

The folding path of the M13 scaffold is more complex in 3D origami structures, with more compact structural characteristics than observed in 2D. Thus, a higher ratio of the unmodified staples to the scaffold (typically 10:1) was used to improve the yield. For the experiments described here we held the ratio between the scaffold and the dye-labeled staples at 1:2 while changing the ratio of M13 to unmodified staples from 1:1, 1:5 to 1:10. We observed a very small difference in the T_f (~ 1 °C), while the T_m was similar for both 1:5 and 1:10 ratios; however, T_f is significantly reduced (5−6°) and the width of the transition is larger (3.3 °C vs 1.2 °C), indicating a much slower formation when there are no excess staples (Table 1B). The melting temperature, T_m, is also significantly lower (2−3°). The 3D origami with a 1:1 ratio of scaffold to staple strands may have some strand mismatches or base-pairs missing at random positions due to a less than 100% yield of the full length staple strands in the synthesis, which is consistent with the result we obtained for the 2D origami. Next we analyzed samples in which the ratio of M13 to dye-modified staples were held at 1:5, while 1:10 and 1:15 ratios of M13 to unmodified staples were tested. Again, similar T_f and T_m values were obtained for both cases (Table 1B). Our results suggest that it is not necessary to use a relatively high molar ratio of M13 to staples for 3D DNA origami structures. However, most reports of 3D DNA origami describe a 1:10 ratio of M13 to staples, and in an effort to remain relevant, we used a 1:2:10 ratio of M13 to dye-modified staples to unmodified staples for experiments with the cuboid structure.

We also evaluated the effect of concentration on origami folding and melting. For 2D origami the transition temperature of folding, T_f, is higher when the concentration is higher and lower when the concentration decreases (Table S6A). This is likely because the staples have a lower probably of encountering and interacting with the scaffold at lower concentrations. However, the transition temperature of melting (dissociation) T_m is similar because the unfolding rate is not affected as much by the concentration. For the 3D origami, the trend in T_f is the same as 2D origami, but the absolute temperature variations are even larger (Table S6B). The T_m was reduced a few degrees when the concentration was decreased. The complicated folding of cuboid origami that more relies on dynamic dissociation and incorporation (on and off rates) may cause this phenomenon. In our study, we chose 50 nM as the standard origami concentration to reduce the impact of hysteresis.

Global Stability of 2D Structures. DNA origami is widely utilized as an addressable scaffold with selected staple strands often modified as target probes or by chemical linkers. Understanding the thermodynamic behavior of DNA origami structures is important to guarantee the stability, integrity, and functionality of the modifications. In this study, we induced various "defects" (staple deletions) to the structures, both close to and far from the FRET reporter dyes, and examined the local and long-range impact of the deletions on the stability of the structures. The inclusion of structural defects and integrity of the resulting structures was confirmed by atomic force microscopy (AFM) (Figure S3).

First we examined the relationship between the two halves of the origami structure that are naturally divided by the folding path of the scaffold. Here, all the staples on the "left" side of the origami were intentionally omitted from the sample mixture such that only the "right" side of the structure (where the FRET dyes are positioned) could form (Figure 3A, left). Compared to the fully assembled reference structure, the transition temperatures of the half origami structure were only ~ 0.1 °C lower, which is within experimental error. This result suggests that the assembly and disassembly of the two halves of the 2D DNA origami rectangle are completely independent of each other, most likely due to the discontinuous arrangement of the scaffold strand across the width of the structure. It is reasonable to conclude that each side of the 2D structure can be manipulated without having an adverse effect on the stability of the other half.

Next, we further omitted groups of staples designed to bind to the scaffold above and below the position of the FRET reporter dyes, leaving a seven-helix core surrounding the fluorophores (Figure 3A, middle). Both transition temperatures (T_f and T_m) decreased by $\sim 0.7-0.9$ °C compared to the fully assembled reference structure, though the shape of the transitions remained the same. The sharp transitions confirm the highly cooperative activity of the staples surrounding the reporter dyes, while the minimal difference in transition temperatures (compared to the reference) suggests that the number of helices in the core is sufficient to maintain the structural integrity of the abbreviated structure.

We went on to delete all but two layers of staples surrounding the FRET dyes (Figure 3A, right). A dramatic 6−7 °C drop (compared to the reference) in both transition temperatures was observed, with a slight broadening of the transition curves. This suggests that the reporter dyes are not sufficiently stabilized by the surrounding double-helical structure and that the self-assembly of the staples is less cooperative. Direct comparison of the scenarios depicted in the middle and right panels of Figure 3A implies that the staples, which are designed to bind to the same stretch of scaffold
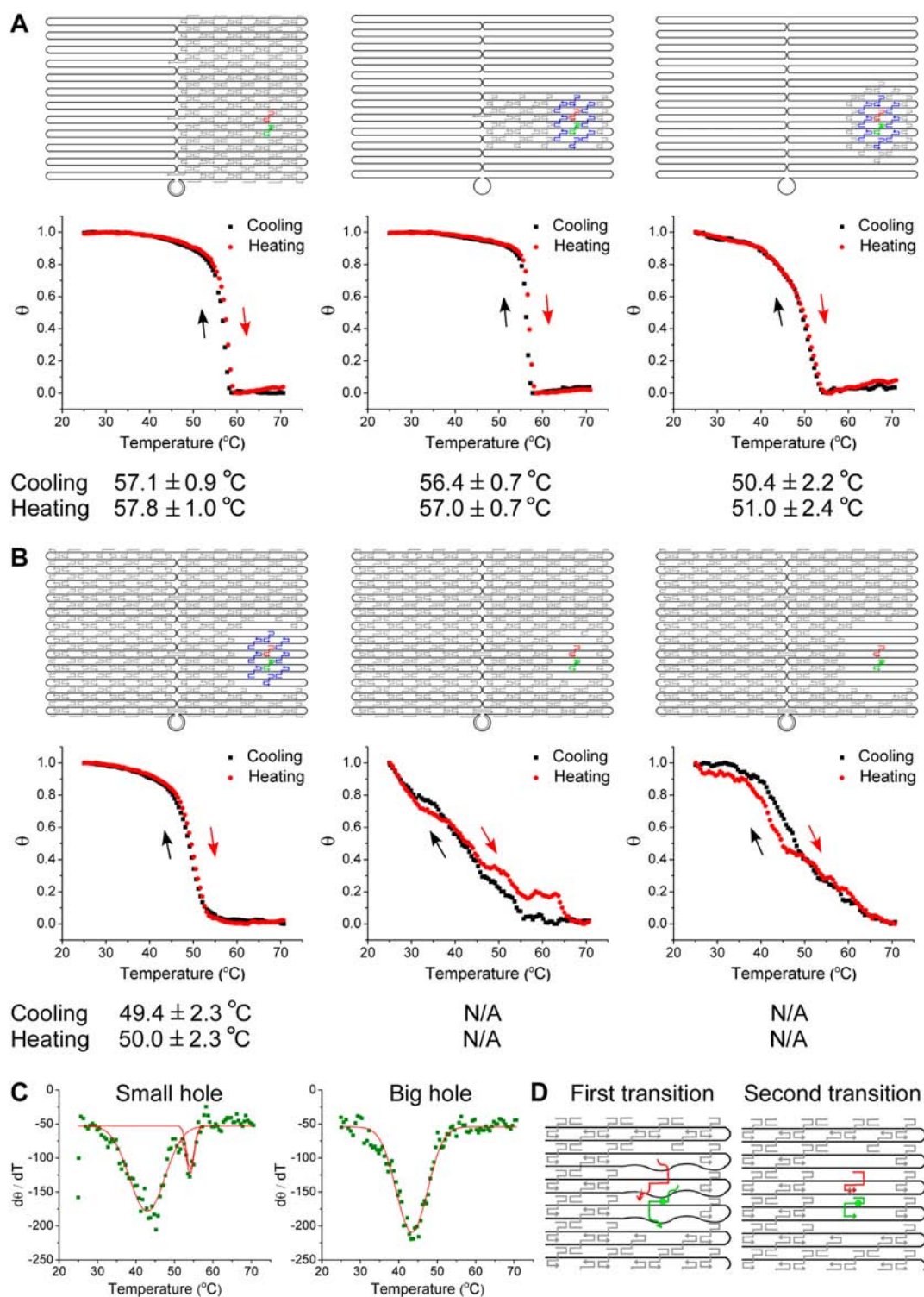
Figure 3. Effect of various structural defects on transition temperatures. For (A) and (B), the upper panels depict the design, while the lower panels present the corresponding thermal melting curves from which the transition temperatures were determined. Note that the position of the reporter dyes is the same for all designs. (A) From left to right: half origami, seven-helix core, and two-layer cluster structures. (B) From left to right: ring-, small-, and big-hole structures. The eight staple strands in the first layer encircling the dyes are highlighted (shown in blue). The transitions corresponding to the small- and big-hole structures could not be reliably fit from the FRET data, so the transition temperatures are not reported here. (C) Plots of the derivative of fluorescence signal of the donor-only sample for the small- and big-hole structures, respectively (cooling cycle, complete data sets are shown in Figures S11 and S12). Gaussian fits of the plots (red lines) yielded transition temperatures of formation (T_f) of 42.9 ± 4.6 and 54.1 ± 1.0 °C for the small-hole structures and 43.4 ± 4.1 °C for the big-hole structure. (D) Proposed model to depict the transitions observed during the cooling cycle.

(along the same helical row) as the reporter dyes, are more important in stabilizing the area than those along other helices.

We subsequently focused on the presence/absence of staples only in the two staple layers immediately encircling the reporter
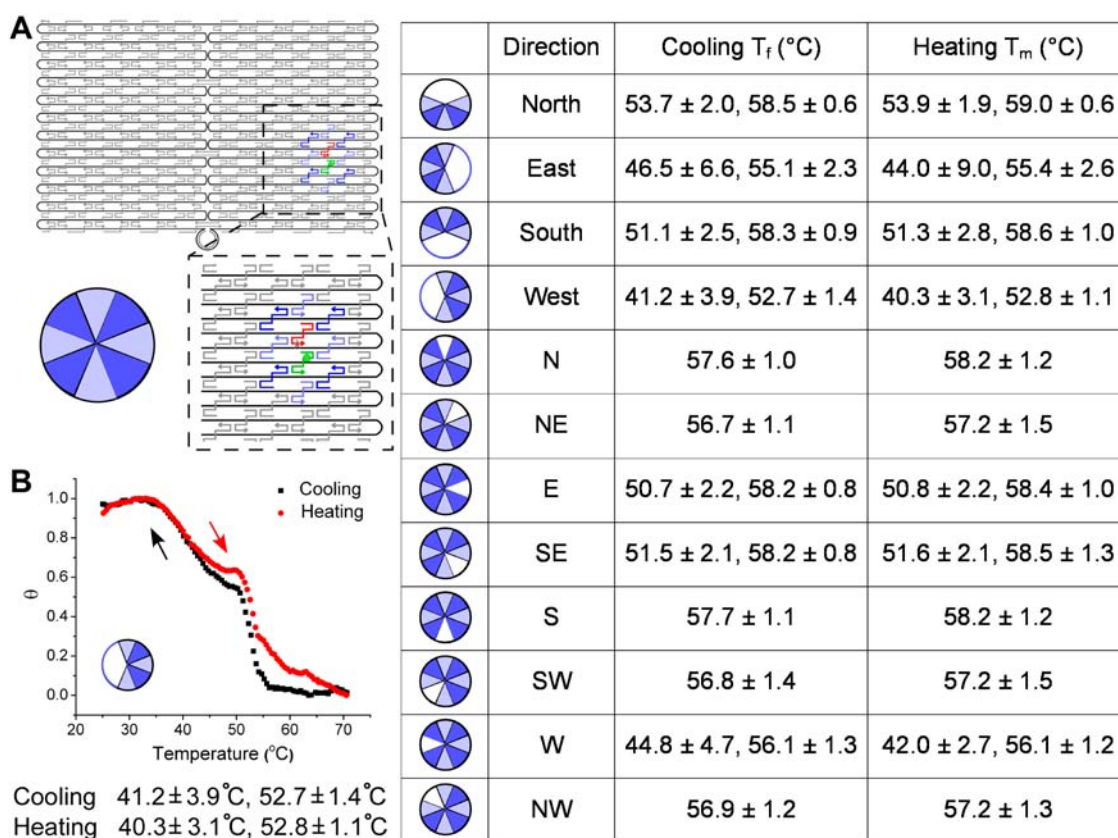
Figure 4. Systematic evaluation of local structural defects. (A) Spotlight on the FRET reporter dye position and the surrounding staples. Note that there are eight staples in the first layer that encircle the dyes (shown in dark and light blue). The staples were selectively omitted one at a time or in clusters of three. In the table on the right, the pie chart depicts the omitted staple(s) position (white slices denote omitted staples). The cardinal direction of the omitted staples is also specified in the table. The remaining two columns in the table correspond to the assembly and melting transition temperatures, respectively. Multiple transitions are listed when applicable. (B) Sample data corresponding to omission of staple cluster W (three staples to the left of the FRET reporter dyes). Two clearly distinguishable transitions are observed in both the cooling and heating cycles.

dyes. We sought to identify how significantly, if at all, do these staples affect the local stability of the structure, and what staples specifically have the largest impact. We examined samples in which the first (8 staples, "small-hole"), second (14 staples, "ring-hole"), or both ("big-hole") layers of staples surrounding the reporter dyes were omitted (Figure 3B). Of the three groups, only the ring-hole sample (first layer of staples surrounding the reporter dyes is present) exhibited sharp, relatively high transition temperatures ~50°C (comparable to the design shown in Figure 3A, right). In the experiments described here, it is apparent that omitting the second layer of staples interferes with the association of the dye-modified strands with the scaffold, possibly due to increased local flexibility.

The other two groups (small- and big-hole structures) exhibited extremely broad transitions ranging from 35 to 50 °C (see complete data set in Figures S11 and S12). Here, the transition temperatures could not be accurately determined due to the smaller amplitude of the fluorescence intensity change compared to the background, an indication that binding equilibrium was not achieved at each temperature. One possible explanation for the low signal-to-noise ratio is related to the flexibility of unpaired regions of the scaffold strand. It is likely that the increased flexibility of the scaffold at positions directly adjacent to the reporter site interferes with the formation of crossovers between adjacent helices and close helical packing, resulting in a larger distance between the FRET dyes.

Fortunately, the donor-only samples corresponding to these groups exhibited more obvious transitions than the fully assembled donor−acceptor samples (Figures 3C and S11 and S12). It should be noted that the position of the donor dye modification is in the middle of the 16 nt long domain of the corresponding staple, not one of the 8 nt terminal domains as is the case for the acceptor dye. Thus, we might expect that the donor-modified staple is subject to more efficient hybridization to the scaffold than the acceptor-modified staple.

A comparison of the donor-only and fully assembled donor−acceptor pair data corresponding to these two samples (small- and big-hole) also supports this explanation (Figures 3C and S11 and S12). For the small-hole design, the donor-only sample exhibited two clear transitions at 42.9 ± 4.6 and 54.1 ± 1.0 °C (cooling cycle). In Figure 3D, the narrower transition observed at ~54 °C can be attributed to the hybridization of the 16 nt long domain of the staples, while the broader transition at ~43 °C reflects hybridization of the two 8 nt domains. In the small-hole design only the first layer of staple strands encircling the reporter site is absent so that the 8 nt staple domains have the opportunity to bind to complementary regions of the scaffold on adjacent helical rows and form crossovers. However, in the big-hole structure there are two layers of absent staples, and a single broad transition is observed 43.4 ± 4.1 °C. In this case it is likely that only the 16 nt domain binds to the scaffold and not the 8 nt domains.

The much lower transition temperatures and broader transition curves for the small- and large-hole structures (compared to the ring-hole structure) indicate that the layer of staples immediately encircling the dye-labeled strands plays a more critical role in stabilizing the local structure than other layers.

Local Stability of 2D Structures. Based on the previous results we further investigated the influence of individual staples surrounding the FRET dyes. A close inspection of Figure 4A reveals the pattern of staples directly adjacent to the reporter site. We distinguished each staple by specifying its cardinal direction (N, NE, E, SE, S, SW, W, and NW) relative to the position of the FRET dyes. We systematically removed each "cardinal" staple one at a time or in groups of three adjacent staples and examined the resulting stability of the structures (Figures 4A and S13−S24).

Omitting staples N or S resulted in no change in the transition temperatures or shape of the transitions (Figures S17 and S21 and data listed in the right table in Figure 4A), as compared to the reference structure. This result was expected as these staples are the most remote from the reporter site, bound to entirely different scaffold rows than the FRET dyes. Removing NE, NW, or SW staples resulted in a ∼ 1 °C drop in the transition temperatures (right table in Figure 4A and S18, S24, and S22). This particular group of staples is designed to bind to the helical scaffold rows directly surrounding the FRET dyes. Defects in these locations may produce a small perturbation to the local thermal stability of the structure.

The result is more complicated when E, SE, and W staples were omitted (right table in Figure 4A and S19, S20, and S23). When E or SE staples were absent two transitions were observed: a small and narrow transition at the same temperature as the reference origami structure (58 °C) and a more dominant, broader transition 6−7 degrees lower (∼51−52 °C). When staple W was omitted, the first transition was 2° lower than the reference (∼56 °C), and the second transition occurred at a drastically lower temperature (∼40 °C). It is important to point out that these three staples bind directly to the same helical row as the FRET dyes. It is evident that a single staple omission at any of these positions directly impacts hybridization of the FRET-modified strands to the scaffold and that centrally located staples (relative to the overall structure) are very important in stabilizing the reporter site (as opposed to those close to the end of the helices).

Generally speaking, we anticipate that omitting a larger number of staples will lead to a more significant decrease in stability. For example, we expect that omitting three staples will be more destabilizing than a single defect. However, it is also important to understand the subtle effects of various defect patterns. For all four cases in which groups of three staples were omitted, two clear transitions were observed (results shown in the right table in Figure 4A, complete data set shown in Figures S13−S16). For example, omitting three staples on the N or S sides of the reporter dyes had a similar effect. A small and sharp transition at 58 °C and a large and slightly broader transition at 51 or 53 °C, respectively, were observed. As shown in Figure 4B, omitting clusters of staples from the E and W sides of the reporter dyes resulted in much broader transitions that were skewed toward lower temperatures (∼50 °C and ∼40 °C for the first and second transition, respectively). Overall, the results here reflect the same trends as were observed for single staple omission experiments.

Mechanism of Assembly in 2D. By comparing the thermal curves corresponding to the donor-only and fully assembled donor−acceptor samples, we were able to develop several hypothesis about the DNA origami assembly process. We theorize that the mechanism proposed in Figure 3D can be used to explain all the observations thus far. For example, consider the situation in which there are staple defects in the area immediately surrounding the reporter site. If one of the omitted staples is designed to bind to the same helical row as the dye-modified staples, then the scaffold strand in the vicinity of the defect is expected to be quite flexible. We propose that during the assembly (cooling) process the dye-modified staples approach the scaffold and hybridize to the complementary domains in a stepwise manner. First, the 16 nt central domain of the staples will bind to the scaffold leaving the two 8 nt terminal domains freely dangling. Here, the FRET donor (fluorescein) is located in the longer central domain, and the initial binding event will be reflected by the increase in fluorescence intensity of the donor-only sample. Simultaneously, binding of the 16 nt domain of the FRET acceptor (TAMRA) modified staple will be echoed by a slight increase in FRET efficiency as the dyes are brought closer together than when they are freely diffusing in solution. As the temperature of the sample is gradually reduced, the flexibility and dynamics of the unbound portions of the scaffold are also reduced, facilitating binding of the remaining 8 nt domains of the dye-modified staples. Finally, the formation of crossovers between neighboring helices fixes the structure, bringing the FRET dyes together for efficient energy transfer. Because the FRET acceptor is located in an 8 nt domain of the corresponding staple, this binding event will be reflected by maximum energy transfer between dyes. In summary, we propose that the first observed transitions reflect binding of longer staple domains, while the second transitions at lower temperatures reflect binding of shorter staple domains. Melting of the assembled structures occurs in a similar manner, with the 8 nt domains of the staples dissociating from the scaffold first, followed by the 16 nt domain at higher temperatures. The presence of multiple transitions for various structures is also explained by a similar mechanism.

Based on this simplified representation of DNA origami assembly and disassembly processes, we expect to observe a single transition in the donor-only samples, as the dye modification is within the longer staple domain that should bind to the scaffold in a single step. However, there were several cases in which multiple transitions were observed. In a few cases (i.e., Figures S19 and S20) two distinct transitions that coincided with those seen in the fully assembled donor−acceptor sample were observed. In all of these situations selected staples directly adjacent to the donor-modified staple were omitted (i.e., cluster S, W, E, or SE).

The appearance of multiple transitions in the donor-only data can be partially explained by the quenching effect of ssDNA on the fluorescence of fluorescein. During the assembly phase, the 16 nt domain of the donor-modified staple binds to the scaffold forming a double helix. This event releases the dye of its interaction with neighboring single-stranded DNA bases which reduces the quenching of the donor's fluorescence and therefore increases the emission of the donor. However, when there is other single-stranded DNA present (either from unpaired sections of the scaffold or dangling domains of other partially bound staples), it also has an opportunity to interact with the donor and partially quench its fluorescence. The
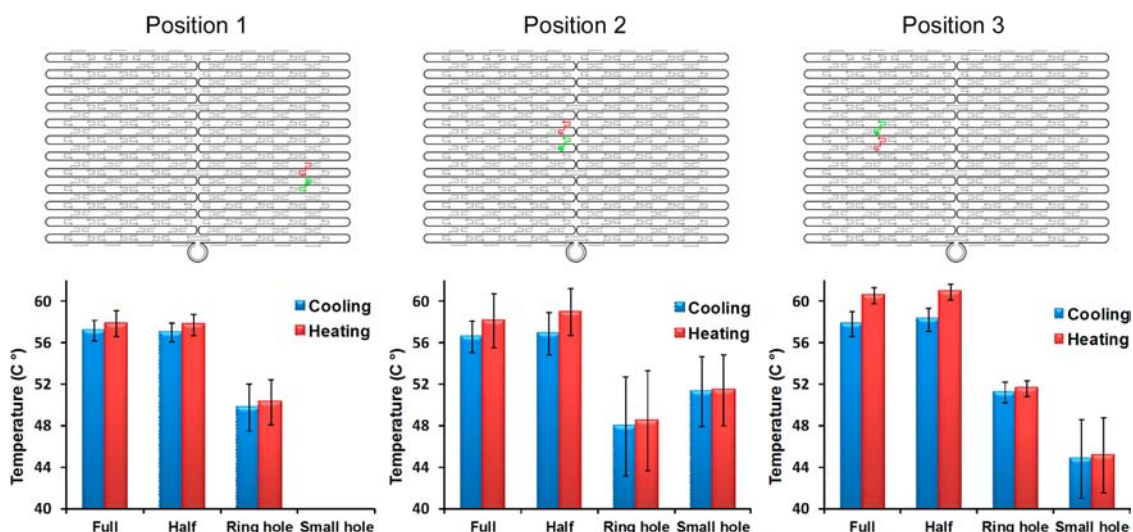
Figure 5. Evaluating the homogeneity of assembly across a 2D rectangular structure. The upper panels show the three different areas that were examined, as indicated by the presence of FRET reporter dyes (shown in green and red). Position 1 is close to the edge in the lower right quadrant (same design as previous study); position 2 is located along the seam created by the scaffold folding path; and position 3 is in the approximate center of the left side of the structure. The lower panels present the transition temperatures corresponding to all the designs investigated (including the reference structure, half origami, ring- and small-hole structures) at each position. All results corresponding to the big- and small-hole structures at position 1 are not presented since they cannot be reliably fit. For those designs that displayed multiple transitions, only the higher temperature one is shown. The error bars represents the transition widths, and the standard deviation of the measurements is much smaller than the transition width. The data is also listed in Table S7.

emission of the donor may undergo a second increase when the dangling domains finally associate with the scaffold and release the dye from any remaining interactions. We also observed three transitions in the donor-only data corresponding to omission of staple cluster S, which is likely the result of similar events.

Interestingly, if the helical rows that the donor-modified staple is bound to are completely surrounded by staples (no omissions), then the second transition was not observed. In those cases binding of the 16 nt domain was not distinguishable from the shorter 8 nt domains. For example, the sample in which cluster N was omitted displayed a single transition at ∼58 °C in the donor-only sample (Figure S13). Meanwhile, a second transition at ∼53 °C was observed for the fully assembled donor−acceptor sample. The second transition is likely due to stepwise binding of the acceptor dye-modified staple rather than the donor-modified staple.

Heterogeneity of Assembly. In all the previously described experiments the dye-modified staples reflected the status of a small area (position 1) in the lower right quadrant of the rectangular structure. To determine if the assembly of the 2D DNA origami rectangle occurs homogeneously across the structure, we also examined several other reporter dye positions (Figure 5). We positioned the dyes along the seam between the two domains of the rectangle (position 2) and also in the center of the left side (position 3). We examined fully assembled structures as references and also simulated several defect states, including the half structure, ring-, small-, and big-hole defects.

The thermal curves corresponding to the fully assembled structures show that position 3 (Figure S30) exhibits the highest T_m (∼61 °C), ∼2.7 °C higher than position 1 (Figure S4) and 2.4 °C higher than position 2 (Figure S25). These results indicate that staples are more easily dissociated from terminal helical positions, rather than interior ones (the seam connects two independent halves, each with helical termini). Thus, melting is likely to be initiated from the far left and right

helical ends and on both sides of the seam. The T_m transition is narrowest at position 3 and broadest at position 2. From this we can speculate that dissociation of staples from the outside layers of the scaffold will cause the M13 in these areas to become progressively more flexible and promote dissociation of the interior staples.

Interestingly, the T_f of the three reference structures differs by less than ∼1 °C (position 3 > position 1 > position 2). Similar to the melting data, the T_f transition is also slightly broader at the seam. Taken together, these results suggest that there exists some form of structural stress along the seam that causes binding to occur more slowly and at a slightly lower temperature than at the other positions. A comparison of the raw cooling data for the three positions shows that the difference between the donor-only and the fully assembled donor−acceptor samples is the smallest at the most shielded position (position 3) while the largest at the seam (position 2). The results indicate that either the assembly yield or the stability of the dye-labeled staples is lowest at the seam.

The transition temperatures of positions 2 and 3 labeled half origami structures reflect a similar trend as position 1, with less than 1 °C difference between the fully and half assembled structures (Figures S26 and S31). This further supports the notion that each side of the rectangular DNA origami structure is independent of the other.

The thermal transitions corresponding to the ring- and small-hole defects at position 3 occur at lower temperatures than at positions 2 and 1 (Table S7 and Figures S32−S33 and S27−S28), when the transitions were reliably fit. This suggests that insulated reporter positions are more sensitive to local structural changes than more accessible ones. Here, the slightly enhanced stability of the region depends on the presence of all the surrounding staples to fix the DNA helices in place. Apparently inducing defects along the edges is less likely to cause damage to the structural integrity of the area than in more centrally located positions.
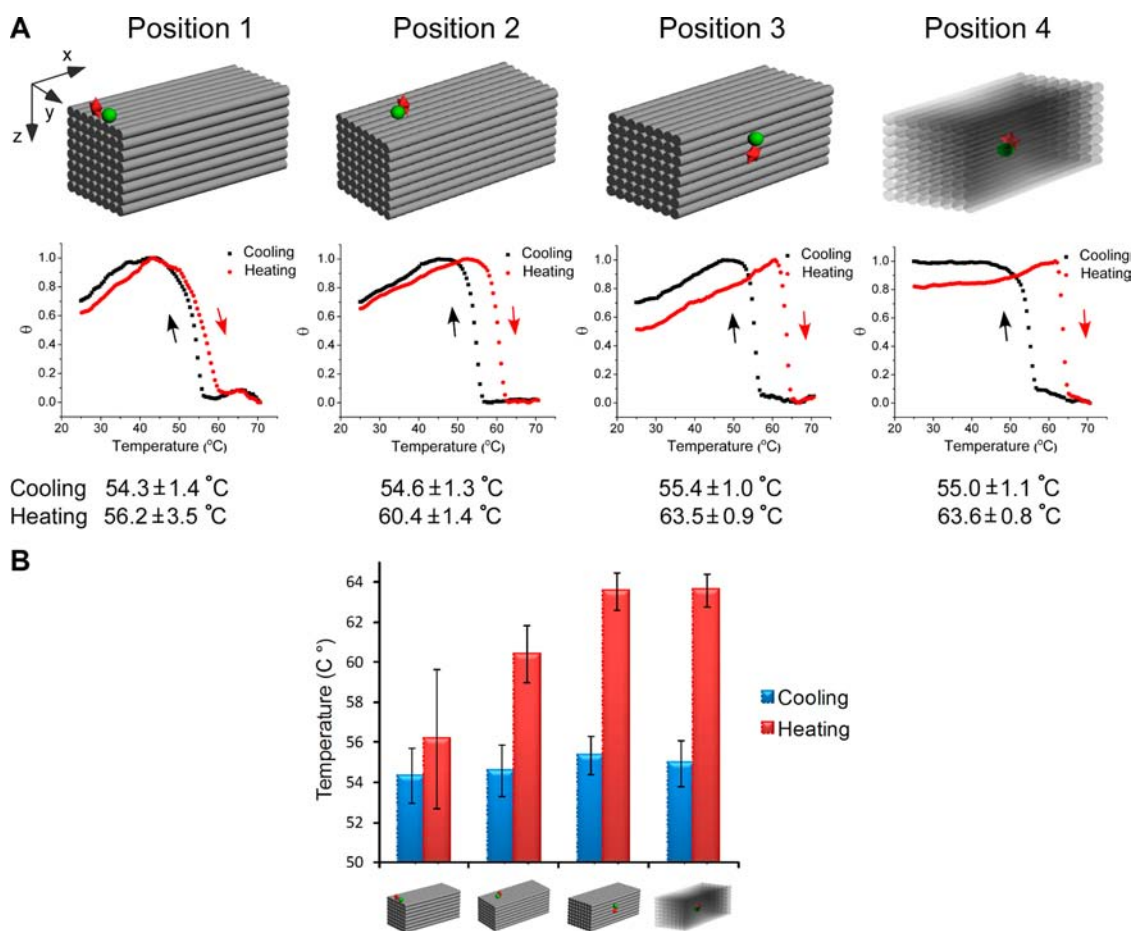
Figure 6. Evaluating the assembly of a 3D cuboid structure. (A) The upper panels show the four different areas of the cuboid that were examined, as indicated by the presence of FRET reporter dyes (shown in green and red). The lower panels present the corresponding thermal transitions during the cooling (black) and heating phases (red). (B) A plot summarizing the transition temperatures of the four positions. The error bars represent the widths of the transitions. No significant difference in T_f was observed among the positions. The T_m was dramatically higher for those positions farthest from the end of the helices.

Assembly in 3D. Our study already demonstrated the extremely reversible and highly cooperative nature of the assembly/disassembly process for 2D DNA origami structures. However, assembling a 3D origami structure, a cuboid for example, not only involves a much more complicated scaffold folding path but also a far more elaborate staple pattern. Many of the staples in 3D structures weave back and forth and bridge more distant helices than in 2D structures. The efficient formation of 3D structures requires more rigorous cooperation among the staples, which is experimentally achieved by annealing for longer times with slower temperature ramps and higher salt concentrations.

We were most interested in monitoring the assembly and disassembly phases at the molecular level. To achieve this we examined four different reporter dye positions within a cuboid structure, reflecting various levels of insulation by other structural elements (Figure 6A). The staples along the length of the cuboid structure are separated into 14 layers (x direction) that are numbered from 1 to 14 (left to right), as shown in Figure 1C. There are 8 helices in the y and z directions, numbered from 1 to 8 from back to front and from top to bottom. The coordinates of the FRET dyes at these four positions are: (2,6,1)-(2,4,1); (3,4,1)-(4,3,1); (6,8,3)-(6,8,5); and (7,4,4)-(6,4,5); respectively, as shown in Figure 6A. The reporter dyes at the first position are fully exposed to solution

at the boundary between the top and the side faces of the structure. The dyes at the second and third positions are slightly less accessible on the top and front face, respectively. The dyes at the last position are buried inside the structure when it is fully assembled (Figure 6A).

The T_f (cooling) corresponding to the four positions vary by only 1°, ranging from 54.3 to 55.4 °C with the more interior positions exhibiting noticeably sharper transitions than the exterior ones. The results suggest that the assembly of 3D origami occurs uniformly across the structure. We surmise that the structure is relatively loose and unstable at temperatures above T_f and forms rapidly at and below the transition temperature in a highly cooperative process of staple hybridization.

However, the T_m (heating) corresponding to the four positions vary widely (Figure 6B). The lowest T_m (56.2 °C) was observed at position 1, indicating that dissociation of the most accessible staples occurs first. The T_m corresponding to position 2, a less exposed position, is 4° higher (60.4 °C). Positions 3 and 4, farthest from the ends of the helices, exhibited melting temperatures ~7° higher (63.5 and 63.6 °C, respectively) than position 1. Thus, it is apparent that dissociation proceeds gradually from the staples closest to the termini of the helices to the innermost positions. The transition curves corresponding to the inner positions are sharper than

those of the outer ones, indicating that the outer staples are not as stable and dissociate more slowly. Note that there is no significant difference in T_m when the reporter dyes are located on staples with the same x-coordinate, regardless of whether or not they are on the surface of the structure or buried in the interior (positions 3 vs 4). Careful examination of the staple binding patterns reveals that the staples with different x-coordinates do not interact with one another, while those with the same x-coordinate participate in crossovers with four to five neighboring helices. This arrangement of staples makes it less likely that melting will proceed in the direction perpendicular to the helical axis.

CONCLUSION

In this study we used a FRET-based method to probe the structural integrity and association/dissociation of DNA origami at the molecular level, unlike other strategies that evaluate average global behavior. The sensitivity and precision of our method allowed us to investigate the influence of scaffold to staple ratios and the presence or absence of staples close to and far from selected reporter sites, on the stability of 2D and 3D structures. We also examined the homogeneity of staple hybridization across entire structures. We observed that the folding and unfolding of 2D structures is very consistent in different areas of the same structure, with evidence of rapid and cooperative staple hybridization. Weak positional effects were observed; more interior positions were more stable, and also more sensitive to local structural defects, than those along the edges and seam. Assembly and disassembly of structures in 3D were not as consistent, with staples at the most accessible positions melting gradually first, followed by rapid dissociation of inner layer staples.

The results draw attention to the importance of scaffold folding paths and staple binding patterns in the thermal stability of origami structures, with a sharp difference in stability observed for unique structural arrangements. This information can be used to guide and optimize the rational design of scaffold folding paths and staple arrangements in more complex DNA nanostructures for high yield and stability.

In addition, the detailed melting behavior that is accessible by our method can be used to tailor annealing protocols for shorter, more efficient assembly conditions. Current annealing protocols often involve heating DNA mixtures to very high temperatures and cooling to room temperature over long periods of time. The results here suggest that it may not be necessary to heat the mixtures to such a high temperature initially, which could be important to DNA systems that involve other more fragile molecules such as folded proteins. Sobczak et al. have already demonstrated the ability to optimize annealing protocols for origami structures by considering temperature.[14] Further studies of the local and global thermal behavior of DNA origami and other DNA nanostructures will facilitate optimization of assembly temperatures and times. Overall, the information gathered from this study can lead to more stable DNA structures with significantly enhanced integrity.

Improving the stability and integrity of DNA origami will allow researchers to effectively modify and functionalize the underlying nanostructures. Understanding how to efficiently and accurately fold and disassemble DNA nanostructures will ultimately improve our ability to manipulate and control such systems.[29−33] This may lead to broader application of the technology.

ASSOCIATED CONTENT

Ⓢ Supporting Information

Detailed descriptions of DNA origami preparation, real-time monitoring of the assembly/disassembly processes, origami designs and DNA sequences, and FRET thermal data processing. This material is available free of charge via the Internet at http://pubs.acs.org.

AUTHOR INFORMATION

Corresponding Author

yan_liu@asu.edu

Notes

The authors declare no competing financial interest.

REFERENCES

(1) Pinheiro, A. V.; Han, D.; Shih, W. M.; Yan, H. *Nat. Nanotechnol.* **2011**, *6*, 763.
(2) Nangreave, J.; Han, D.; Liu, Y.; Yan, H. *Curr. Opin. Chem. Biol.* **2010**, *14*, 608.
(3) Seeman, N. C. *Mol. Biotechnol.* **2007**, *37*, 246.
(4) Rothemund, P. W. *Nature* **2006**, *440*, 297.
(5) Dietz, H.; Douglas, S. M.; Shih, W. M. *Science* **2009**, *325*, 725.
(6) Douglas, S. M.; Dietz, H.; Liedl, T.; Hogberg, B.; Graf, F.; Shih, W. M. *Nature* **2009**, *459*, 414.
(7) Gu, H.; Chao, J.; Xiao, S. J.; Seeman, N. C. *Nat. Nanotechnol.* **2009**, *4*, 245.
(8) Seeman, N. C. *Annu. Rev. Biochem.* **2010**, *79*, 65.
(9) Castro, C. E.; Kilchherr, F.; Kim, D. N.; Shiao, E. L.; Wauer, T.; Wortmann, P.; Bathe, M.; Dietz, H. *Nat. Methods* **2011**, *8*, 221.
(10) Sobey, T. L.; Renner, S.; Simmel, F. C. *J. Phys.: Condens. Matter* **2009**, *21*, 034112.
(11) Rajendran, A.; Endo, M.; Katsuda, Y.; Hidaka, K.; Sugiyama, H. *J. Am. Chem. Soc.* **2011**, *133*, 14488.
(12) Mergny, J. L.; Lacroix, L. *Oligonucleotides* **2003**, *13*, 515.
(13) Song, J.; Arbona, J. M.; Zhang, Z.; Liu, L.; Xie, E.; Elezgaray, J.; Aime, J. P.; Gothelf, K. V.; Besenbacher, F.; Dong, M. *J. Am. Chem. Soc.* **2012**, *134*, 9844.
(14) Sobczak, J. P. J.; Martin, T. G.; Gerling, T.; Dietz, H. *Science* **2012**, *338*, 1458.
(15) Forster, T. *Discuss. Faraday Soc.* **1959**, *27*, 7.
(16) Lilley, D. M. J.; Wilson, T. J. *Curr. Opin. Chem. Biol.* **2000**, *4*, 507.
(17) Liedl, T.; Simmel, F. C. *Anal. Chem.* **2007**, *79*, 5212.
(18) Stein, I. H.; Schuller, V.; Bohm, P.; Tinnefeld, P.; Liedl, T. *Chem. Phys. Chem* **2011**, *12*, 689.
(19) Sacca, B.; Meyer, R.; Feldkamp, U.; Schroeder, H.; Niemeyer, C. M. *Angew. Chem., Int. Ed.* **2008**, *47*, 2135.
(20) Sacca, B.; Meyer, R.; Niemeyer, C. M. *Nat. Protoc.* **2009**, *4*, 271.
(21) Nangreave, J.; Yan, H.; Liu, Y. *Biophys. J.* **2009**, *97*, 563.
(22) Nangreave, J.; Yan, H.; Liu, Y. *J. Am. Chem. Soc.* **2011**, *133*, 4490.
(23) Dacres, H.; Wang, J.; Dumancic, M. M.; Trowell, S. C. *Anal. Chem.* **2010**, *82*, 432.
(24) Ke, Y.; Douglas, S. M.; Liu, M.; Sharma, J.; Cheng, A.; Leung, A.; Liu, Y.; Shih, W. M.; Yan, H. *J. Am. Chem. Soc.* **2009**, *131*, 15903.
(25) Bowen, E. J.; Sahu, J. *J. Phys. Chem.* **1959**, *63*, 4.
(26) You, Y.; Tataurov, A. V.; Owczarzy, R. *Biopolymers* **2011**, *95*, 472.
(27) Sjoback, R.; Nygren, J.; Kubista, M. *Biopolymers* **1998**, *46*, 445.

(28) Pinheiro, A. V.; Nangreave, J.; Jiang, S.; Yan, H.; Liu, Y. *ACS Nano* **2012**, *6*, 5521.

(29) Deng, Z.; Samanta, A.; Nangreave, J.; Yan, H.; Liu, Y. *J. Am. Chem. Soc.* **2012**, *134*, 17424.

(30) Ding, B.; Wu, H.; Xu, W.; Zhao, Z.; Liu, Y.; Yu, H.; Yan, H. *Nano Lett.* **2010**, *10*, 5065.

(31) Pal, S.; Deng, Z.; Ding, B.; Yan, H.; Liu, Y. *Angew. Chem., Int. Ed.* **2010**, *49*, 2700.

(32) Bell, N. A.; Engst, C. R.; Ablay, M.; Divitini, G.; Ducati, C.; Liedl, T.; Keyser, U. F. *Nano Lett.* **2012**, *12*, 512.

(33) Douglas, S. M.; Bachelet, I.; Church, G. M. *Science* **2012**, *335*, 831.

6176

dx.doi.org/10.1021/ja4000728 | *J. Am. Chem. Soc.* 2013, 135, 6165–6176